coatings

MDPI

Article

Influence of Parameters in LDH Preparation on Its Morphology Structure and Corrosion Protection Property

Jingjing Wang [1,2], Shuyou Luo [2,3], Kaifeng Chen [2,*], Yanhui Cao [2,*], Lingwei Ma [3,*] and Dawei Zhang [3]

[1] College of Chemistry and Chemical Engineering, Xiamen University, Xiamen 361005, China; jingjing811014@163.com
[2] National Key Laboratory of Marine Corrosion and Protection, Luoyang Ship Material Research Institute, Xiamen 361101, China; luoshuyou200010@163.com
[3] Institute for Advanced Materials and Technology, University of Science and Technology Beijing, Beijing 100083, China; dzhang@ustb.edu.cn
* Correspondence: xm725ckf@163.com (K.C.); yanhuicao@vip.163.com (Y.C.); mlw1215@ustb.edu.cn (L.M.)

Abstract

Layered double hydroxide (LDH) has been widely used in the field of corrosion protection. LDH nanofillers can act as multifunctional additives in coatings based on the physical barrier effect and anion exchange effect. However, the preparation of the typical co-precipitation method needs to be simplified to realize large-scale industrialization. In this work, a wide range of synthesis parameters, including solution-mixing mode, reaction atmosphere, reaction pH control, titration rate and post-treatment on the obtained LDH, were systematically studied, and it was found that the one-step solution-mixing synthesis procedure and the adoption of N_2 atmosphere were able to alleviate the carbonate contamination to some degree. However, the one-step solution-mixing synthesis procedure has a negative influence on the formation of LDH, probably due to insufficient reaction, while the hydrothermal post-treatment is able to promote the continual growth of the LDH platelet and, thus, lead to an increase in crystallinity and particle size. Green inhibitor aspartates were used to modify LDH, and the electrochemical test results indicated that the adoption of N_2 atmosphere was able to clearly increase the corrosion protection ability of LDH, with an R_p value of 3.86 kΩ·cm^2 after immersion for 96 h in 0.1 mol/L NaCl, probably due to the intercalation of a relatively large amount of inhibitor anions since less carbonates were intercalated, followed by the LDH synthesized via co-precipitation without N_2 protection, pH control and hydrothermal post-treatment with an R_p value of 3.00 kΩ·cm^2. The LDH sample without inhibitor intercalation presented a corresponding R_p value of 2.45 kΩ·cm^2. Notably, the one-step solution-mixing method and a fast titration rate in co-precipitation would have a negative influence on the corrosion protection of LDH, probably due to insufficient reaction. This work could shed light on the simplification of LDH preparation, and it is able to provide a solid foundation and technical support for the wide promotion and application of LDH in anti-corrosion and other fields in the near future.

Keywords: layered double hydroxide; co-precipitation; synthesis parameter; corrosion protection; industrialization

Check for updates

Academic Editor: Stefano Caporali

Received: 21 May 2026
Revised: 13 July 2026
Accepted: 15 July 2026
Published: 20 July 2026

Copyright: © 2026 by the authors. Licensee MDPI, Basel, Switzerland. This article is an open access article distributed under the terms and conditions of the Creative Commons Attribution (CC BY) license.

1. Introduction

Coatings have been widely used for corrosion protection of metals over recent decades. The permeation of an aggressive medium through the coating is able to cause the initiation of corrosion at the interface of metal and coatings. Therefore, the efforts concerning the

prevention of the transportation of a corrosive medium in coatings have been devoted by researchers in recent years to increasing the service life of the coatings [1,2]. The development and application of nanofillers in the form of two-dimensional platelets could significantly contribute to the physical barrier effect of the coatings, which would prevent the permeation of aggressive medium in the coatings by increasing tortuosity. This was also called the labyrinth effect in the coatings. On the other hand, many nanofillers can be regarded as inhibitor containers, and inhibitors can be released on demand simultaneously, such as metal–organic framework (MOF) [3], graphene oxide (GO) [4], MXene [5,6], SiO_2 microsphere [7] and layered double hydroxide (LDH) [8]. In this case, the system was able to present self-healing properties.

LDH can be used as nanofillers in anti-corrosion coatings through both of the above-mentioned mechanisms, including the physical barrier effect and the self-healing effect. LDH presented hexagonal-shaped platelets, and it was composed of hydroxide layers and intercalated anions in the interlayer space. As some divalent metal cations were replaced by some trivalent metal cations, the hydroxide layers were positively charged. Thus, negatively charged anions were needed in the gallery to balance the extra positive charges [9–11]. It is worth noting that the intercalated anions were able to have an anion exchange reaction with the anions in the environment such as the aggressive chlorides. As a result, the concentration of chlorides was reduced, and the corrosion inhibitors could be released into the environment simultaneously [12,13]. Therefore, LDH can be used as a unique functional filler in coatings based on the above physical barrier effect, chloride-trapping effect and inhibitor-releasing effect. It has been widely investigated and applied in anti-corrosion coatings by researchers worldwide.

Various LDHs with two different metal cations, such as ZnAl-LDH, MgAl-LDH and CaAl-LDH, etc., were synthesized and reported. It was reported by Cao et al. that CaAl-LDH presented better corrosion protection ability in comparison with the other two LDHs due to the better compatibility with the coating matrix when no corrosion inhibitors were intercalated [14]. Mohammad Tabish et al. used 2-mercaptobenzothiazole (MBT) to modify CaAl-LDH, and it was found that the usage of 2% in the epoxy coating was able to present a significant enhancement in corrosion protection, mainly due to the release of MBT and formation of a chelate network caused by the reaction between MBT and Fe^{2+} [15]. Furthermore, Wang et al. prepared CaAl-LDH intercalated with three kinds of aromatic inhibitors and evaluated their corrosion protection in epoxy coatings. The results indicated that MBT-intercalated CaAl-LDH demonstrated superior corrosion protection in comparison with the other two LDHs intercalated with sodium benzoate (BZ) and benzotriazole (BTA) due to the physical adsorption, chemical adsorption and anti-bonding effect [16]. Andrea Cristoforetti et al. prepared sebacate intercalated CaAl layered double-hydroxide pigments, and they investigated the anion exchange between nitrates and chlorides using total nitrogen analysis. The improvement in corrosion protection was due to the release of sebacate, which was accompanied by partial dissolution caused by alkalinization [17]. Li et al. synthesized CaAl LDH intercalated with L-cysteine and its derivatives, and it was found that LDH modified by the S-benzyl-L-cysteine exhibited more excellent corrosion resistance performance due to its larger molecular volume and also an increase in the thickness of LDH [18].

The typical preparation methods of LDH include the co-precipitation method, anion exchange method and calcination reconstruction method [19]. It should be noted that the co-precipitation method is the most frequently used method for preparation due to relatively high crystallinity. This process involves titration of the salt solution with corresponding metal cations to alkaline solution. However, it should be noted that nitrogen gas is usually used as the protection inert gas to avoid the contamination of CO_2 since

carbonates have strong affinity with LDH interlayers [20,21]. In addition, after the co-precipitation process, the LDH slurry is usually transferred to the hydrothermal reactor for hydrothermal reaction to obtain LDH with high crystallinity and quality [14]. In addition, in a typical co-precipitation procedure, the pH of the reaction solution is usually measured and controlled to a constant value [22]. The above-mentioned preparation conditions indicated the complexity of the co-precipitation method, and the simplification of the process was needed to realize its wide industrialization. Until now, the impact of inert gas protection, the control of pH, the titration speed and also the hydrothermal post-treatment on the morphology, structure and corrosion protection ability of LDH have never been investigated, which will provide significant guidance on the simplification of the co-precipitation method to promote its large-scale industrial production. In addition, a green corrosion inhibitor of aspartate was used to modify CaAl-LDH in this work to further promote its corrosion protection effect concerning the higher environmental protection requirements nowadays.

Thus, in this work, a wide range of synthesis parameters, as mentioned above, in the co-precipitation method were varied, and the obtained CaAl-LDH was characterized comprehensively in terms of morphology and structure. In addition, inhibitors of aspartate were intercalated into LDH though the anion exchange method to study the changes in its corrosion protection ability. This work mainly focused on the investigation of the influence of parameter variations on the morphology, structure and corrosion protection property of LDH, hence simplifying the preparation procedure of LDH to promote the large-scale industrial production and widen its application in anti-corrosion coatings, which is totally different from the above-mentioned work published previously. The relationship between the property characteristics, including morphology, structure, corrosion protection and the corresponding synthesis parameters, was presented, and the in-depth underlying mechanism was elucidated from the micro level. This work can shed light on the optimization of LDH preparation in the promotion of industrialization and provide inspiring insight for related engineers in the field of corrosion protection.

2. Materials and Methods

2.1. Materials

Aluminum nitrate ($Al(NO_3)_3 \cdot 9H_2O$), calcium nitrate ($Ca(NO_3)_2 \cdot 4H_2O$), sodium hydroxide (NaOH), sodium nitrate ($NaNO_3$) and sodium tartrate (TA) were purchased from Sinopharm Chemical Reagent Co., Ltd. (Beijing, China). Aspartic acid (Asp) was supplied by Sinopharm Chemical Reagent Co., Ltd. (Shanghai, China). The deionized water was used for solution preparation. Q235 carbon steel was provided by Xiamen Qianfeng Mechanical Co., Ltd., (Xiamen, China).

2.2. Preparation of LDH Samples

2.2.1. Synthesis of LDH

Solution A was prepared as a mixed solution containing 0.5 mol/L $Ca(NO_3)_2 \cdot 4H_2O$ and 0.25 mol/L $Al(NO_3)_3 \cdot 9H_2O$. Solution B was prepared as a mixed solution containing 2 mol/L $NaNO_3$ and 3 mol/L NaOH. At room temperature (25 ± 5) °C, 200 mL of solution A was added dropwise to 100 mL of solution B at a titration rate of one drop per second, and the mixed solution was vigorously stirred during the titration process at a stirring speed of 600 rpm. After all of solution A had been titrated into solution B, continuous stirring was maintained for an additional 20 min. The resulting slurry was then sealed in the beaker and subjected to hydrothermal reaction in an oven at 65 °C for 24 h. Afterward, the mixture was centrifuged at 8000 rpm for 5 min, followed by three washes with deionized water.

The obtained solid was dried in an oven at 65 °C for 48 h. The final product was designated as LDH-1. A schematic illustration of LDH-1 synthesis process is shown in Figure 1.

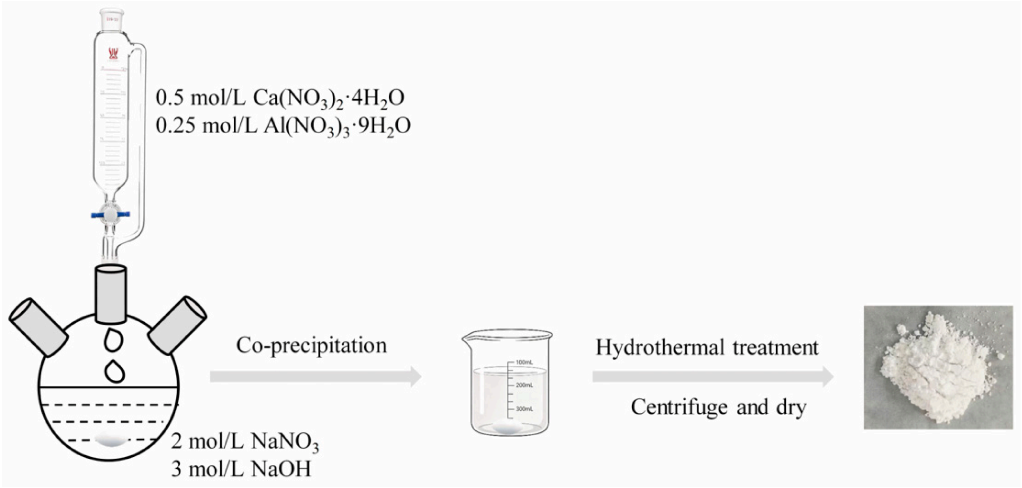


Figure 1. The schematic diagram of the preparation process.

2.2.2. Synthesis of LDHs with Different Preparation Processes

Solution-mixing method: In the LDH preparation process of the above experiment, solution A was added dropwise into solution B. According to literature research, some researchers directly mixed the two solutions. Therefore, 200 mL of solution A was mixed with 100 mL of solution B directly, and then it was subjected to ultrasonication for 20 min followed by vigorous stirring for 20 min (stirring speed of 600 rpm). The other preparation procedures were the same as those in the preparation of LDH-1. The product of this experiment was denoted as LDH-2.

Reaction atmosphere: In the preparation process of LDH-1, as described above, titration was carried out under air. However, CO_2 in the air can dissolve in water to form CO_3^{2-}, and CO_3^{2-} has strong affinity with LDH layer, making it difficult for many corrosion inhibitor anions to replace the interlayer CO_3^{2-} and resulting in a reduced loading amount. Therefore, in this experiment, N_2 was used as protection gas during titration, and the product was denoted as LDH-3.

Reaction process pH: In the above experiment, no operation was carried out to maintain a constant pH during this process. Some research results involved real-time pH monitoring and constant control during mixing of the two solutions. Therefore, 3 mol/L NaOH solution was used to adjust the pH of the mixed solution to 12.0 ± 0.5 during the titration process in this experiment. The other preparation procedures were the same as those in the preparation of LDH-1. The product was labelled as LDH-4.

Titration rate: The titration rate in the LDH preparation process of the above experiment was one drop per second. Thus, 200 mL of solution A was titrated into 100 mL of solution B at a rate of two drops per second in this experiment, and the other preparation procedures were the same as those in the preparation of LDH-1. The product was denoted as LDH-5.

Post-hydrothermal treatment: In the above experiment, the LDH aging treatment was carried out at 65 °C under normal pressure in a beaker. In this experiment, the mixed slurry was transferred into a stainless hydrothermal reactor at 65 °C under high pressure, and the obtained product was denoted as LDH-6.

2.2.3. Synthesis of LDH with Corrosion Inhibitor

Here, 100 mL of 0.1 mol/L aspartic acid solution was prepared, and 0.8 g of solid NaOH was added for deprotonation treatment; then, the pH was adjusted to 11.0 ± 0.5 by

adding an appropriate amount of 3 mol/L NaOH solution. Then, 1 g of LDH-1 was added to aspartate solution, and the solution was stirred at room temperature for 24 h at a speed of 500 rpm. Then, the target product could be obtained via centrifugation at 8000 rpm for 5 min. Finally, the product was washed three times with deionized water and dried at 65 °C for 48 h. The product was named as LDH-A1.

2.3. Characterization

The surface morphology of the samples was examined using a scanning electron microscope (SEM, ZEISS ULTRA55, Carl Zeiss AG Co., Ltd., Dresden, Germany). Elemental analysis and elemental mapping were performed with an energy-dispersive X-ray spectroscopy system (EDS, Carl Zeiss AG Co., Ltd., Dresden, Germany) at an accelerating voltage of 20 kV. The chemical composition of the composite filler was analyzed by Fourier-transform infrared spectroscopy (FTIR, Nicolet iS20, Thermo Fisher Scientific Co., Ltd., Waltham, MA, USA) within a wavenumber range of 400–4000 cm^{-1}. The crystalline structure of samples was characterized by X-ray diffraction (XRD, X'Pert PRO, Malvern PANalytical Co., Ltd., Almelo, The Netherlands) with a scanning range of 5–80° and a scan rate of 10°/min. The carbon steel after immersion in NaCl solution was observed using an optical microscope (LeicaDVM6, Leica Microsystems, Wetzlar, Germany).

2.4. Anti-Corrosion Performance Test

The electrochemical impedance spectroscopy (EIS) measurements for bare steel immersion were conducted using an Autolab electrochemical workstation (Metrohm China Limited, Beijing, China) with a three-electrode system configuration, where carbon steel with an exposed area of 1 cm^2 served as working electrode, an Ag/AgCl electrode worked as reference electrode and a platinum sheet electrode worked as counter electrode. Before electrochemical test, carbon steel samples were sandblasted using sandpaper with grades 400, 800,1200 and 1500, respectively. After that, the samples were washed ultrasonically in ethanol for 10 min and dried in ambient atmosphere naturally. The frequency range was set from 10^5 to 10^{-2} Hz with a sinusoidal perturbation amplitude of 10 mV. There are 5 frequency points per decade. Thus, 100 mL 0.1 mol/L sodium chloride solution was employed as corrosive medium with LDH content of 5 g/L. Three parallel samples were used for EIS tests to ensure reproducibility. The software Zview 3.0a was used for EIS data fitting.

3. Results and Discussion

3.1. Characterization of LDH

Figure 2a presents the XRD patterns of LDH samples prepared via different synthesis processes. As shown in the figure, characteristic diffraction peaks of CaAl-LDH appeared in LDH samples prepared via different fabrication processes. Three main diffraction peaks were observed at 10.34°, 20.64° and 31.19°, which corresponded to the (003), (006) and (012) crystal planes of LDH (JCPDS#89-6723), respectively [14,15,23]. The position of the (003) plane peak suggested that nitrates mainly accounted for the intercalated anions. As for the sample of LDH-2 synthesized via the one-pot solution-mixing method, the intensity of the peak corresponding to the (003) plane decreased remarkably. This phenomenon was probably due to insufficient reaction during the quick mixing procedure. In addition, when the hydrothermal reactor was used for the aging treatment, the diffraction intensity of the characteristic diffraction peaks of LDH-6 increased significantly. According to the Scherrer equation (Eq1), the crystallite size of LDH-6 would be increased upon the increase in crystallinity, indicating that high pressure during aging treatment led to an increase in the crystallite size of LDH. The above results demonstrated that the variation in preparation

parameters was able to cause some changes in the crystallinity of LDH. It can be seen that post-hydrothermal treatment could increase the crystallinity of LDH greatly, while the one-step solution-mixing method had a negative influence on the crystalline structure of LDH.

$$D = \frac{K\lambda}{\beta \cos \theta} \quad (1)$$

D is the grain size, K is the Scherrer constant, λ is the X-ray wavelength, β is the half-peak width corresponding to the diffraction peak and θ is the corresponding diffraction angle.

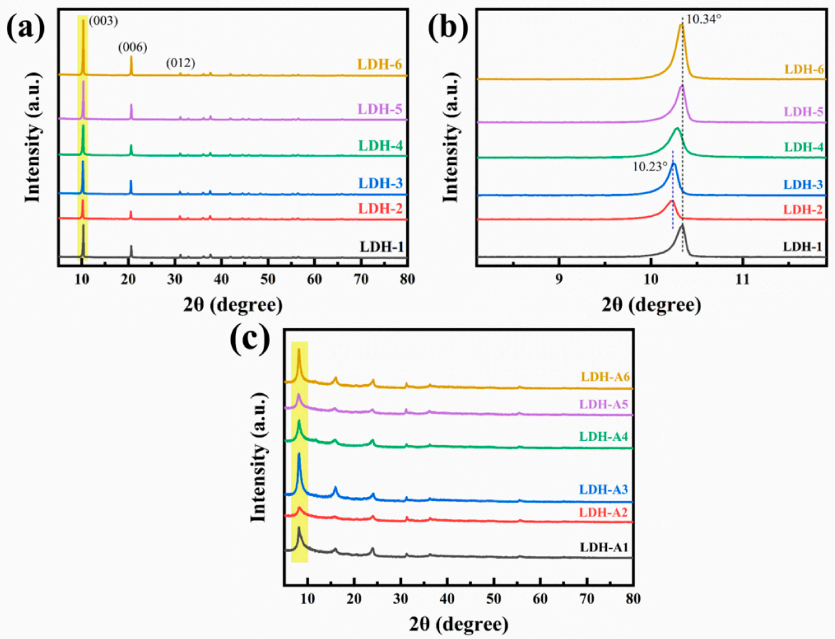


Figure 2. XRD patterns: (**a**) LDH samples prepared via different preparation processes, (**b**) magnified view of 8–12° for (**a**), (**c**) LDH samples intercalated with aspartate prepared via different preparation processes.

Furthermore, Figure 2b presents a magnification of the region ranging from 8° to 11° in Figure 2a. As can be observed from the figure, the diffraction peaks of the (003) crystal planes of LDH-2 and LDH-3 were shifted slightly from 10.34° to 10.23°. Based on the Bragg equation, the interlayer spacing of LDH-2 and LDH-3 was increased from 0.855 nm to 0.864 nm, which was probably attributed to the reduction in interlayer CO_3^{2-} content. CO_2 in the air dissolved into the solution to form CO_3^{2-}. The ionic size of CO_3^{2-} was smaller than that of NO_3^-, and the binding of CO_3^{2-} to LDH lamellae was stronger than that of NO_3^-. Both the one-pot mixing preparation procedure and the adoption of N_2 as the protection inert gas could lead to less contact of the solution with CO_2 in ambient atmosphere. As a result, the interlayer distance of LDH-2 and LDH-3 was higher than other LDHs. The above result indicated that the one-step solution mixing method and adoption of N_2 protection atmosphere would have some influence on the composition of the intercalated anions of LDH, which would decrease the content of the intercalated carbonates.

A green corrosion inhibitor of aspartate was selected to investigate the structural changes in LDH samples prepared via different parameters during intercalation of corrosion inhibitor anions. As shown in Figure 2c, the (003) crystal plane diffraction peak of all the LDH samples shifted significantly to the left after aspartate intercalation, indicating that aspartates had been successfully intercalated into the interlayer of LDH samples. The characteristic diffraction peaks of aspartate-intercalated LDH samples prepared via

different processes all appeared at the same position, demonstrating that changing the preparation process had no significant effect on the following anion exchange reaction of LDH in various inhibitor solutions.

Figure 3 presents morphologies of LDH samples fabricated via different preparation processes characterized by SEM. As shown in the figure, all LDH samples prepared by different processes exhibited a typical sheet-like hexagonal structure, and most of the samples presented a platelet size ranging from approximately 1 μm to 5 μm. Notably, LDH-6 presented LDH platelets with a larger size in comparison with other samples, and the biggest platelets can exceed 5 μm, which was probably due to the continual growth of crystalline particles during the hydrothermal treatment in a hydrothermal reactor. Correspondingly, the intensity of the (003) peak in the XRD diagram increased remarkably in comparison with other samples, indicating the improved crystallinity of this sample. In addition, more irregular platelets appeared in the SEM of LDH-2, which was in good accordance with the decreased crystallinity of LDH-2 in Figure 2a. This result indicated that the direct solution-mixing method to prepare LDH would have a negative effect on its formation, while the post-hydrothermal treatment could enlarge the size of the LDH particles to some extent, and other parameter variations, including the reaction atmosphere, pH of the solution and titration rate, could not influence the particle size and morphology of the formed LDH.

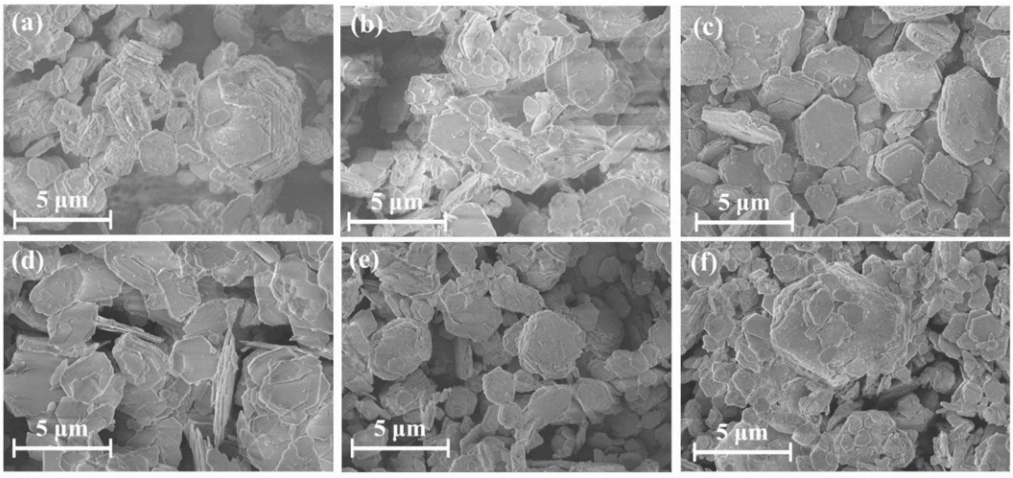


Figure 3. Morphology images of LDH samples prepared via different preparation processes: (**a**) LDH-1, (**b**) LDH-2, (**c**) LDH-3, (**d**) LDH-4, (**e**) LDH-5, (**f**) LDH-6.

Figure 4 shows the morphology of LDH samples intercalated with aspartate based on LDH prepared via different processes. It could be observed that all LDH samples obtained via different preparation processes exhibited a typical hexagonal structure, and the agglomeration was significantly alleviated compared with that before aspartate intercalation. This indicated that aspartate intercalation did not exert a significant influence on the morphology of LDH samples prepared via different preparation processes, and aspartate can improve the dispersion of LDH to some extent.

Figure 5a presents the FTIR results of LDH samples prepared via different synthesis processes. All LDH samples exhibited a broad absorption band near 3469 cm^{-1}, which was assigned to the stretching vibration of O-H groups in the interlayer of LDH and the vibration of physically adsorbed water molecules [12]. The absorption peak at 1645 cm^{-1} was associated with the H-O-H stretching vibration [13]. The absorption bands observed in the range of 500–800 cm^{-1} were assigned to the M-O and M-OH lattice vibrations of the LDH layers, where M = Ca, Al [16,24]. The strong absorption peak of the LDH samples near 1400 cm^{-1} corresponded to the symmetric stretching vibration of NO_3^-, and the additional

absorption peak near 1345 cm^{-1} was attributed to the stretching vibration of CO_3^{2-}, which originated from the contamination of CO_2 in ambient air and deionized water during the preparation process [25]. The above results indicated that the preparation process did not exert a significant effect on the chemical composition of LDH.

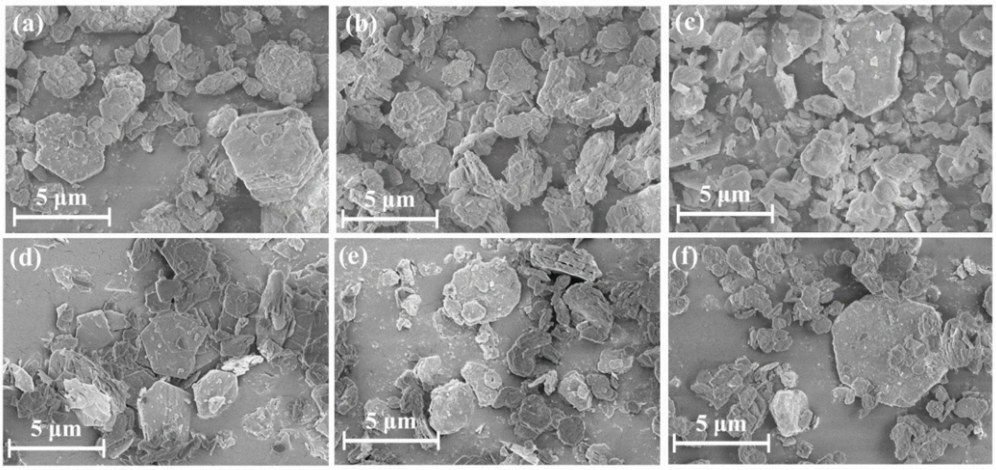


Figure 4. Morphology images of LDH samples intercalated with aspartate based on LDH prepared via different preparation processes: (**a**) LDH-A1, (**b**) LDH-A2, (**c**) LDH-A3, (**d**) LDH-A4, (**e**) LDH-A5, (**f**) LDH-A6.

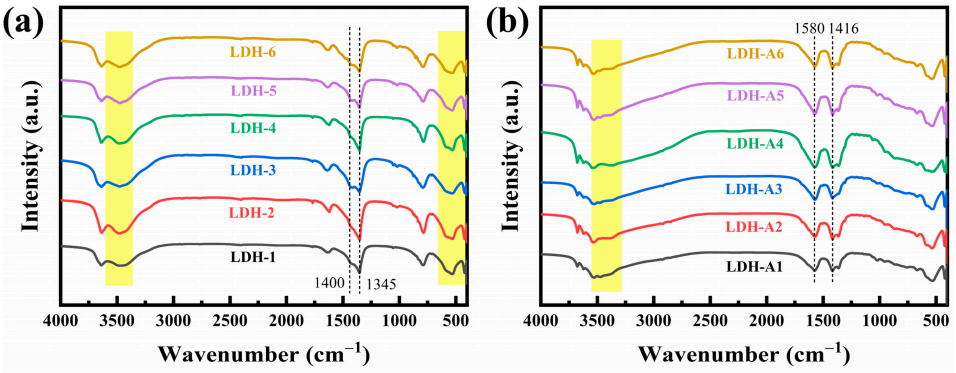


Figure 5. FTIR spectra of (**a**) LDH samples prepared via different preparation processes; (**b**) LDH samples intercalated with aspartate based on LDH prepared via different preparation processes.

Figure 5b presents the FTIR spectra of aspartate-intercalated LDH samples prepared via different synthesis processes. The strong peak 1416 cm^{-1} was assigned to the symmetric stretching vibrations of the carboxylate group (-COO^-) in aspartate. An obvious shoulder peak near 1580 cm^{-1} was attributed to the bending vibration of -NH_2 in aspartate. It can be seen that the FTIR spectra of aspartate-intercalated LDH samples prepared via different synthesis processes all exhibited the characteristic absorption peaks of both LDH and aspartate, indicating that aspartate anions had been successfully loaded in LDH, and variations in the preparation process did not affect the chemical composition of the resulting material.

3.2. Anti-Corrosion Effect of Various LDH Samples

In order to improve the corrosion protection ability of the synthesized LDH, the corrosion inhibitor of aspartate was used to modify LDH to realize environmental friendliness due to the strict environmental protection standard in practical applications. The EIS tests were performed to evaluate the corrosion protection effect. For comparison, the EIS tests in blank NaCl solutions without and with LDH containing no inhibitors were also

carried out. Figure 6 shows the EIS plots of Q235 carbon steel electrodes after immersion in different test solutions for 1 h, 4 h, 8 h, 24 h, 48 h, 72 h, 96 h and 120 h, respectively. The left panel presents Nyquist plots, and the right panel presents Bode plots. All the Nyquist plots present only one capacitive arc. In Bode plots, the impedance modulus at 0.01 Hz ($|Z|_{0.01Hz}$) was commonly employed to evaluate the corrosion inhibition capability of corrosion inhibitors on metals. The $|Z|_{0.01Hz}$ value of carbon steel in blank solutions remained in the order of 10^3 Ω·cm^2 throughout the entire immersion period, indicating that severe corrosion occurred on the carbon steel surface. After immersion in the LDH-1 test solution, the $|Z|_{0.01Hz}$ of carbon steel decreased from 1.11×10^5 Ω·cm^2 (after 1 h) to 9.74×10^3 Ω·cm^2 (after 120 h). This phenomenon can be attributed to the ion exchange capacity of LDH, which adsorbed part of Cl^- in the solution into the interlayer region and released NO_3^- at the same time, thereby mitigating the corrosion of carbon steel [13].

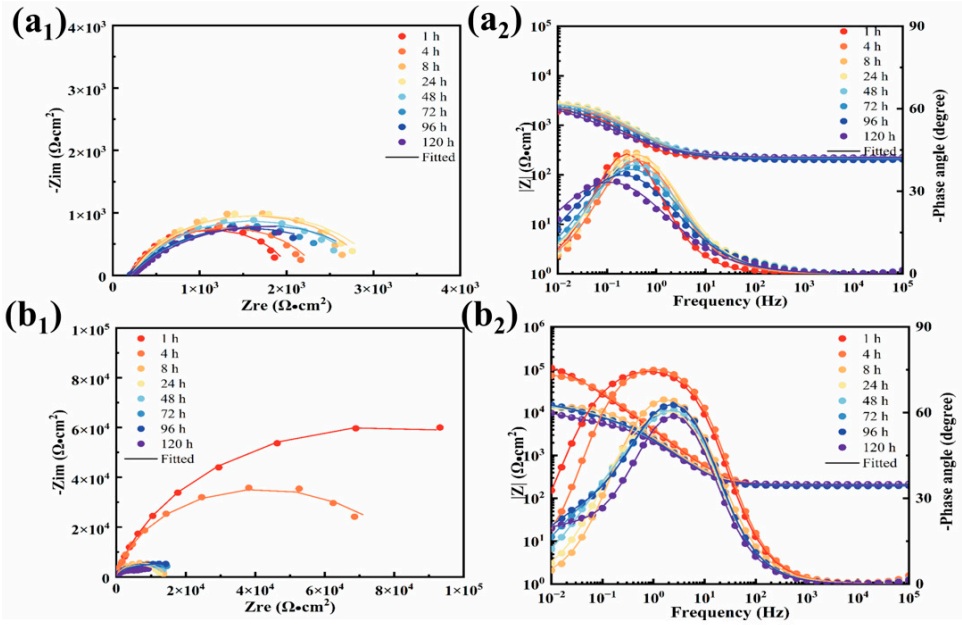


Figure 6. EIS results of Q235 carbon steel immersed in different solutions containing (**a$_1$**,**a$_2$**) blank, (**b$_1$**,**b$_2$**) LDH-1.

When Q235 carbon steel was immersed in blank NaCl solution, its Nyquist plot only presented one capacitive arc, so this system could be fitted by an equivalent circuit with one time constant in Figure 7a corresponding to the electrochemical corrosion process. When Q235 carbon steel was immersed in the test solution containing various LDH, a broad phase angle peak could be observed in the Bode plots during the initial immersion period. The peak became narrowed with the increased immersion, and a small peak appeared at lower frequencies. According to the reported literature [26,27], the protective layer in the form of a passivation film caused by high alkalinity or adsorption of inhibitor molecules was able to lead to the presence of another time constant in the EIS diagram in addition to the time constant related to the electrochemical corrosion process. In the case of LDH-1, a passive film could be formed in situ on the carbon steel surface in strongly alkaline solutions due to the hydroxyl-releasing behavior of LDH, as evidenced in our previous work [16]. Therefore, the equivalent circuit shown in Figure 7b with two time constants was adopted to fit the EIS results.

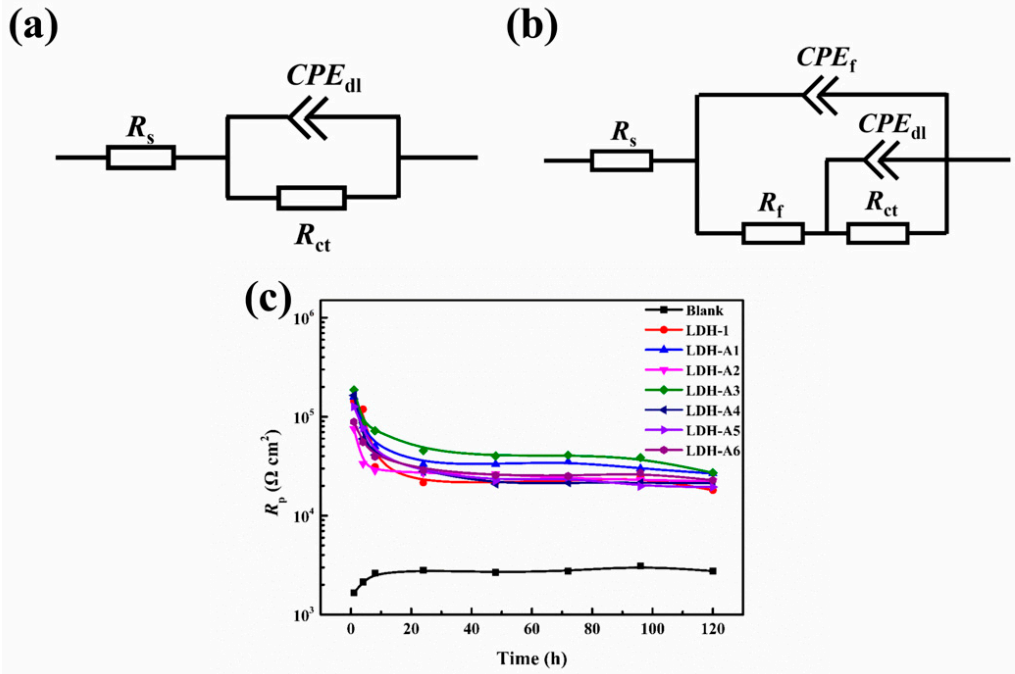


Figure 7. (**a**,**b**) Equivalent circuit used for fitting EIS results; (**c**) R_p variation curves of carbon steel in test solutions with inhibitor anion-intercalated LDH samples.

Figure 8 presents the EIS results of LDH-A1, where the left panel of the figure shows a Nyquist plot and the right panel shows a Bode plot. As illustrated in the figure, in the test solution of LDH intercalated with aspartate prepared via different synthesis processes, a single capacitive arc was observed in all systems during immersion. After carbon steel was immersed in the test solutions of LDH-A1 for 120 h, the $|Z|_{0.01Hz}$ values were 2.32×10^4 Ω·cm^2, which was an improvement to some extent compared with the $|Z|_{0.01Hz}$ value of carbon steel immersed in the LDH-1 test solution. This could be attributed to the fact that the corrosion inhibitor anions of aspartates intercalated in the LDH layers could undergo ion exchange with Cl^- in the solution to achieve controlled release. In addition, the released corrosion inhibitor anions of aspartates migrated to the carbon steel interface and formed a protective barrier film with coordination-like stability based on the fact that the heteroatoms of aspartates such as N and O participated in the donor–acceptor interaction with the vacant d-orbitals of Fe atoms at the surface, thereby inhibiting the electrochemical corrosion process of the substrate [28,29]. In the Bode plots, a broad phase angle peak appeared in the initial immersion period, and it narrowed with increased immersion. The appearance of the broad phase angle peak can be attributed to the overlapping of two peaks. The equivalent circuit with two time constants can be used to fit the EIS data, where one time constant corresponded to the formed film on the surface and the other corresponded to the electrochemical corrosion process. The appearance of the wide phase angle peak was due to the overlapping of the two phase angle peaks corresponding to the protective film and the corrosion process, respectively. However, as the immersion time increased, the protective film was damaged, allowing the corrosive medium to directly erode the carbon steel. In this case, the two phase angle peaks can be observed more clearly. Thus, the equivalent circuit shown in Figure 7b with two time constants was also adopted to fit the EIS results.

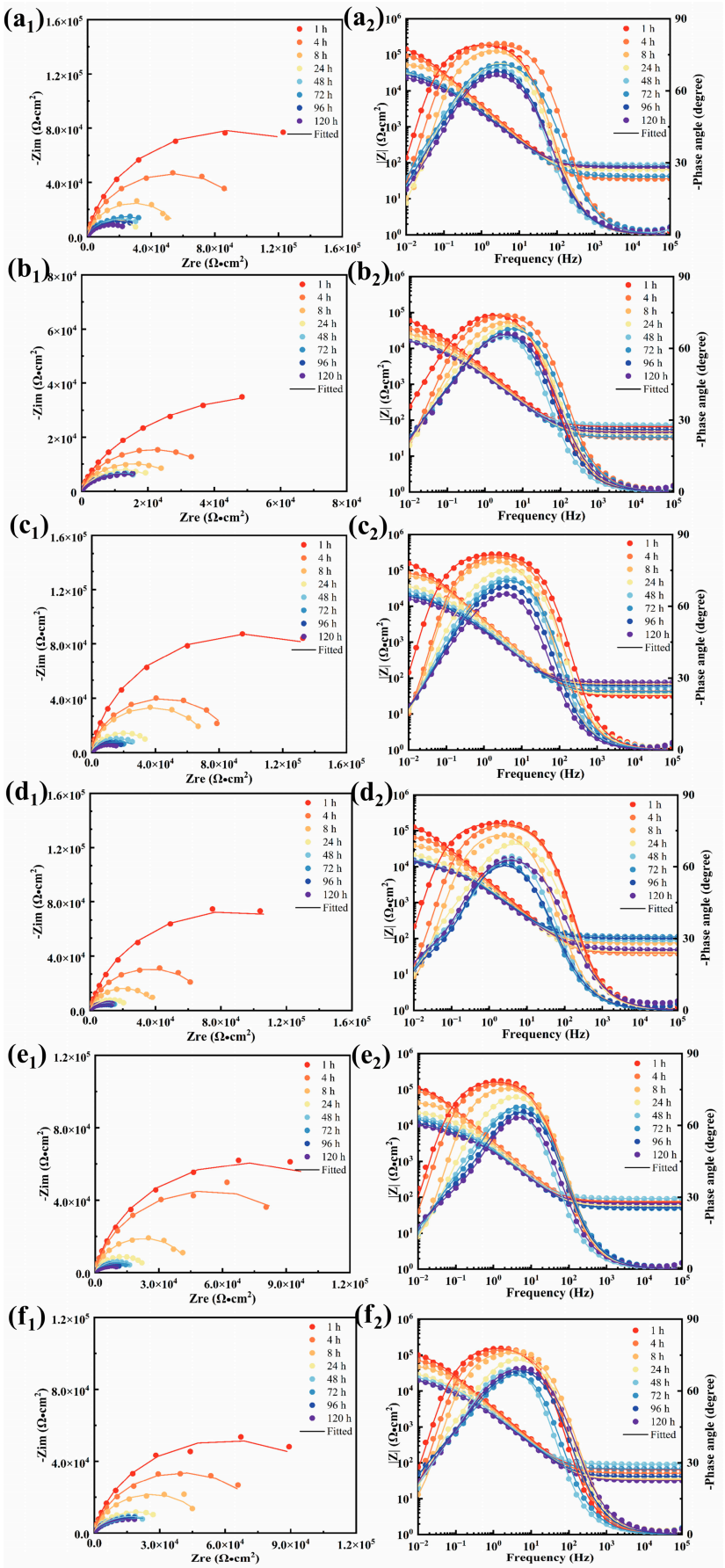


Figure 8. EIS results of Q235 carbon steel immersed in test solutions of ($\mathbf{a_1}$,$\mathbf{a_2}$) LDH-A1, ($\mathbf{b_1}$,$\mathbf{b_2}$) LDH-A2, ($\mathbf{c_1}$,$\mathbf{c_2}$) LDH-A3, ($\mathbf{d_1}$,$\mathbf{d_2}$) LDH-A4, ($\mathbf{e_1}$,$\mathbf{e_2}$) LDH-A5, ($\mathbf{f_1}$,$\mathbf{f_2}$) LDH-A6.

In the equivalent circuit in Figure 7a,b, R_s denotes the solution resistance, R_f represents the film resistance, CPE_f stands for the film capacitance, R_{ct} and CPE_{dl} are parameters associated with the electrochemical corrosion process at the interface between the solution and the carbon steel electrode surface, corresponding to the charge transfer resistance and the double-layer capacitance, respectively. The corresponding fitting results are presented in Tables 1 and 2.

Table 1. The parameters obtained from the fitting of the EIS data in Figure 6.

Samples	Immersion Time	CPE_f		R_f ($\Omega \cdot cm^2$)	CPE_{dl}		R_{ct} ($\Omega \cdot cm^2$)	Chi-Square Value (χ^2)
		Y_f ($\Omega^{-1} \cdot cm^{-2} \cdot s^n$)	n_f		Y_{dl} ($\Omega^{-1} \cdot cm^{-2} \cdot s^n$)	n_{dl}		
Blank	1 h	—	—	—	$(1.06 \pm 0.12) \times 10^{-3}$	0.83	$(1.66 + 0.20) \times 10^3$	6.0×10^{-3}
	4 h	—	—	—	$(7.60 + 1.37) \times 10^{-4}$	0.80	$(2.14 + 0.13) \times 10^3$	1.6×10^{-2}
	8 h	—	—	—	$(7.10 + 1.32) \times 10^{-4}$	0.78	$(2.63 + 0.30) \times 10^3$	1.7×10^{-2}
	24 h	—	—	—	$(6.97 + 0.75) \times 10^{-4}$	0.75	$(2.81 + 0.19) \times 10^3$	1.5×10^{-2}
	48 h	—	—	—	$(7.92 + 0.58) \times 10^{-4}$	0.73	$(2.67 + 0.32) \times 10^3$	1.0×10^{-2}
	72 h	—	—	—	$(9.92 + 1.44) \times 10^{-4}$	0.67	$(2.76 + 0.30) \times 10^3$	2.1×10^{-3}
	96 h	—	—	—	$(1.19 + 0.19) \times 10^{-3}$	0.64	$(3.10 + 0.91) \times 10^3$	2.4×10^{-3}
	120 h	—	—	—	$(1.40 + 0.23) \times 10^{-3}$	0.62	$(2.76 + 0.35) \times 10^3$	1.9×10^{-3}
LDH-1	1 h	$(5.40 + 0.34) \times 10^{-5}$	0.90	$(6.62 + 2.55) \times 10^4$	$(2.30 + 1.26) \times 10^{-4}$	0.98	$(7.68 + 3.95) \times 10^4$	1.8×10^{-4}
	4 h	$(5.44 + 0.49) \times 10^{-5}$	0.90	$(7.03 + 1.69) \times 10^4$	$(5.83 + 6.29) \times 10^{-5}$	0.95	$(4.86 + 2.24) \times 10^4$	4.3×10^{-4}
	8 h	$(5.70 + 0.50) \times 10^{-5}$	0.90	$(2.09 + 1.27) \times 10^4$	$(6.43 + 3.64) \times 10^{-5}$	0.94	$(1.02 + 1.15) \times 10^4$	1.2×10^{-3}
	24 h	$(6.19 + 0.96) \times 10^{-5}$	0.90	$(5.99 + 0.38) \times 10^3$	$(1.30 + 0.27) \times 10^{-4}$	0.77	$(1.56 + 1.15) \times 10^4$	7.0×10^{-4}
	48 h	$(6.75 + 0.77) \times 10^{-5}$	0.88	$(4.99 + 0.77) \times 10^3$	$(2.32 + 0.42) \times 10^{-4}$	0.74	$(1.67 + 0.90) \times 10^4$	1.8×10^{-3}
	72 h	$(6.96 + 1.20) \times 10^{-5}$	0.88	$(5.16 + 2.10) \times 10^3$	$(3.05 + 0.77) \times 10^{-4}$	0.68	$(1.73 + 0.69) \times 10^4$	1.1×10^{-3}
	96 h	$(7.44 + 1.23) \times 10^{-5}$	0.87	$(4.83 + 2.22) \times 10^3$	$(3.77 + 0.93) \times 10^{-4}$	0.65	$(1.97 + 0.31) \times 10^4$	1.3×10^{-3}
	120 h	$(7.44 + 1.28) \times 10^{-5}$	0.87	$(3.11 + 0.10) \times 10^3$	$(4.45 + 1.03) \times 10^{-4}$	0.60	$(1.50 + 0.87) \times 10^4$	1.4×10^{-3}

Table 2. The parameters obtained from the fitting of the EIS data in Figure 8.

Samples	Immersion Time	CPE_f		R_f ($\Omega \cdot cm^2$)	CPE_{dl}		R_{ct} ($\Omega \cdot cm^2$)	Chi-Square Value (χ^2)
		Y_f ($\Omega^{-1} \cdot cm^{-2} \cdot s^n$)	n_f		Y_{dl} ($\Omega^{-1} \cdot cm^{-2} \cdot s^n$)	n_{dl}		
LDH-A1	1 h	$(4.66 \pm 0.23) \times 10^{-5}$	0.91	$(1.32 \pm 0.48) \times 10^5$	$(4.11 \pm 3.36) \times 10^{-4}$	0.90	$(2.70 \pm 1.91) \times 10^4$	2.3×10^{-3}
	4 h	$(5.00 \pm 0.68) \times 10^{-5}$	0.91	$(5.85 \pm 2.88) \times 10^4$	$(8.21 \pm 8.38) \times 10^{-5}$	0.77	$(2.20 \pm 1.44) \times 10^4$	1.6×10^{-3}
	8 h	$(5.47 \pm 0.57) \times 10^{-5}$	0.90	$(3.09 \pm 1.33) \times 10^4$	$(5.26 \pm 1.67) \times 10^{-5}$	0.88	$(1.93 \pm 0.25) \times 10^4$	1.2×10^{-3}
	24 h	$(6.83 \pm 1.06) \times 10^{-5}$	0.87	$(1.50 \pm 0.60) \times 10^4$	$(1.31 \pm 0.53) \times 10^{-4}$	0.81	$(1.81 \pm 0.42) \times 10^4$	1.4×10^{-3}
	48 h	$(7.08 \pm 0.57) \times 10^{-5}$	0.88	$(1.30 \pm 0.45) \times 10^4$	$(1.85 + 0.71) \times 10^{-4}$	0.73	$(2.02 + 0.30) \times 10^4$	1.1×10^{-3}
	72 h	$(7.47 + 0.37) \times 10^{-5}$	0.86	$(1.50 + 0.86) \times 10^4$	$(2.66 + 0.68) \times 10^{-4}$	0.76	$(2.02 + 0.15) \times 10^4$	1.7×10^{-3}
	96 h	$(7.88 + 0.23) \times 10^{-5}$	0.85	$(1.14 + 0.48) \times 10^4$	$(2.73 + 1.15) \times 10^{-4}$	0.71	$(1.86 + 0.20) \times 10^4$	2.0×10^{-3}
	120 h	$(8.6 + 0.74) \times 10^{-5}$	0.83	$(1.16 + 0.61) \times 10^4$	$(3.84 + 1.10) \times 10^{-4}$	0.71	$(1.51 + 0.57) \times 10^4$	1.2×10^{-3}
LDH-A2	1 h	$(7.32 + 0.14) \times 10^{-5}$	0.87	$(2.00 + 1.39) \times 10^4$	$(1.24 + 0.75) \times 10^{-4}$	0.52	$(5.52 + 3.58) \times 10^4$	7.7×10^{-4}
	4 h	$(8.44 + 0.13) \times 10^{-5}$	0.87	$(1.17 + 1.16) \times 10^4$	$(1.38 + 1.12) \times 10^{-4}$	0.52	$(2.18 + 0.64) \times 10^4$	1.2×10^{-3}
	8 h	$(8.98 + 0.27) \times 10^{-5}$	0.87	$(6.66 + 3.36) \times 10^3$	$(1.47 + 0.88) \times 10^{-4}$	0.55	$(2.19 + 0.16) \times 10^4$	1.0×10^{-3}
	24 h	$(1.00 + 0.00) \times 10^{-4}$	0.86	$(6.28 + 3.25) \times 10^3$	$(2.04 + 0.41) \times 10^{-4}$	0.55	$(2.08 + 0.68) \times 10^4$	1.2×10^{-3}
	48 h	$(1.02 + 0.05) \times 10^{-4}$	0.85	$(4.48 + 1.89) \times 10^3$	$(2.07 + 0.54) \times 10^{-4}$	0.55	$(2.18 + 0.45) \times 10^4$	8.8×10^{-4}
	72 h	$(1.12 + 0.08) \times 10^{-4}$	0.85	$(4.56 + 1.49) \times 10^3$	$(2.34 + 0.89) \times 10^{-4}$	0.55	$(1.93 + 0.23) \times 10^4$	1.0×10^{-3}
	96 h	$(1.17 + 0.04) \times 10^{-4}$	0.84	$(5.04 + 2.28) \times 10^3$	$(2.62 + 0.93) \times 10^{-4}$	0.57	$(1.80 + 0.06) \times 10^4$	1.5×10^{-3}
	120 h	$(1.23 + 0.08) \times 10^{-4}$	0.82	$(5.92 + 2.92) \times 10^3$	$(3.12 + 0.69) \times 10^{-4}$	0.61	$(1.63 + 0.25) \times 10^4$	1.5×10^{-3}
LDH-A3	1 h	$(4.30 + 0.05) \times 10^{-5}$	0.93	$(1.50 + 0.26) \times 10^5$	$(7.68 + 3.54) \times 10^{-5}$	0.98	$(3.67 + 0.95) \times 10^4$	1.8×10^{-4}
	4 h	$(4.43 + 0.18) \times 10^{-5}$	0.93	$(6.68 + 1.45) \times 10^4$	$(1.51 + 1.90) \times 10^{-4}$	0.94	$(1.99 + 1.70) \times 10^4$	1.3×10^{-4}
	8 h	$(4.82 + 0.11) \times 10^{-5}$	0.92	$(5.63 + 1.30) \times 10^4$	$(7.16 + 1.75) \times 10^{-5}$	0.80	$(1.58 + 0.79) \times 10^4$	1.5×10^{-3}
	24 h	$(6.07 + 0.52) \times 10^{-5}$	0.89	$(2.32 + 0.61) \times 10^4$	$(8.49 + 0.13) \times 10^{-5}$	0.72	$(2.22 + 0.18) \times 10^4$	1.2×10^{-3}
	48 h	$(6.62 + 0.57) \times 10^{-5}$	0.89	$(1.41 + 0.60) \times 10^4$	$(8.33 + 0.37) \times 10^{-5}$	0.64	$(2.60 + 0.38) \times 10^4$	8.3×10^{-4}
	72 h	$(7.49 + 1.12) \times 10^{-5}$	0.87	$(1.51 + 0.86) \times 10^4$	$(1.06 + 0.30) \times 10^{-4}$	0.58	$(2.57 + 1.10) \times 10^4$	1.6×10^{-3}
	96 h	$(7.80 + 0.91) \times 10^{-5}$	0.87	$(1.17 + 0.74) \times 10^4$	$(9.13 + 2.02) \times 10^{-5}$	0.56	$(2.69 + 1.16) \times 10^4$	8.6×10^{-4}
	120 h	$(8.81 + 0.42) \times 10^{-5}$	0.86	$(8.26 + 4.48) \times 10^3$	$(1.29 + 0.10) \times 10^{-4}$	0.57	$(1.88 + 0.31) \times 10^4$	8.2×10^{-4}
LDH-A4	1 h	$(5.02 + 0.02) \times 10^{-5}$	0.90	$(1.20 + 0.34) \times 10^5$	$(7.12 + 3.31) \times 10^{-5}$	0.89	$(4.43 + 2.06) \times 10^4$	2.6×10^{-3}
	4 h	$(5.64 + 0.12) \times 10^{-5}$	0.90	$(4.18 + 1.75) \times 10^4$	$(7.08 + 3.46) \times 10^{-5}$	0.87	$(1.80 + 0.49) \times 10^4$	2.2×10^{-3}
	8 h	$(6.20 + 0.21) \times 10^{-5}$	0.89	$(2.07 + 0.17) \times 10^4$	$(6.55 + 1.15) \times 10^{-5}$	0.84	$(2.03 + 0.08) \times 10^4$	1.4×10^{-3}
	24 h	$(7.50 + 0.68) \times 10^{-5}$	0.87	$(1.06 + 0.15) \times 10^4$	$(1.90 + 0.39) \times 10^{-4}$	0.78	$(1.74 + 0.58) \times 10^4$	2.1×10^{-3}
	48 h	$(8.58 + 0.67) \times 10^{-5}$	0.85	$(8.11 + 0.89) \times 10^3$	$(3.39 + 0.78) \times 10^{-4}$	0.78	$(1.28 + 0.47) \times 10^4$	1.2×10^{-3}
	72 h	$(9.09 + 0.74) \times 10^{-5}$	0.83	$(8.79 + 0.16) \times 10^3$	$(5.40 + 3.10) \times 10^{-4}$	0.78	$(1.27 + 0.49) \times 10^4$	1.3×10^{-3}
	96 h	$(9.58 + 1.06) \times 10^{-5}$	0.82	$(8.71 + 0.22) \times 10^3$	$(6.83 + 5.54) \times 10^{-4}$	0.78	$(1.28 + 0.64) \times 10^4$	1.0×10^{-3}
	120 h	$(1.02 + 0.13) \times 10^{-4}$	0.81	$(8.37 + 0.38) \times 10^3$	$(7.00 + 4.14) \times 10^{-4}$	0.75	$(1.29 + 0.50) \times 10^4$	1.5×10^{-3}

Table 2. *Cont.*

Samples	Immersion Time	CPE_f		R_f ($\Omega \cdot cm^2$)	CPE_{dl}		R_{ct} ($\Omega \cdot cm^2$)	Chi-Square Value (χ^2)
		Y_f ($\Omega^{-1} \cdot cm^{-2} \cdot s^n$)	n_f		Y_{dl} ($\Omega^{-1} \cdot cm^{-2} \cdot s^n$)	n_{dl}		
LDH-A5	1 h	$(5.72 + 0.75) \times 10^{-5}$	0.90	$(6.36 + 3.51) \times 10^4$	$(6.64 + 5.03) \times 10^{-5}$	0.50	$(6.30 + 3.25) \times 10^4$	1.2×10^{-3}
	4 h	$(5.97 + 0.97) \times 10^{-5}$	0.90	$(4.73 + 3.32) \times 10^4$	$(8.47 + 6.91) \times 10^{-5}$	0.67	$(2.95 + 1.86) \times 10^4$	1.6×10^{-3}
	8 h	$(6.50 + 0.56) \times 10^{-5}$	0.89	$(2.22 + 0.60) \times 10^4$	$(7.73 + 6.70) \times 10^{-5}$	0.71	$(1.86 + 0.20) \times 10^4$	1.2×10^{-3}
	24 h	$(7.55 + 0.23) \times 10^{-5}$	0.88	$(1.25 + 0.19) \times 10^4$	$(1.48 + 0.64) \times 10^{-4}$	0.70	$(1.53 + 0.11) \times 10^4$	1.7×10^{-3}
	48 h	$(8.38 + 0.25) \times 10^{-5}$	0.87	$(9.84 + 2.74) \times 10^3$	$(2.30 + 0.37) \times 10^{-4}$	0.72	$(1.26 + 0.11) \times 10^4$	1.4×10^{-3}
	72 h	$(8.45 + 0.70) \times 10^{-5}$	0.87	$(8.51 + 2.88) \times 10^3$	$(2.29 + 0.39) \times 10^{-4}$	0.63	$(1.59 + 0.63) \times 10^4$	1.7×10^{-3}
	96 h	$(9.16 + 0.35) \times 10^{-5}$	0.86	$(7.18 + 3.78) \times 10^3$	$(2.63 + 0.37) \times 10^{-4}$	0.61	$(1.26 + 0.21) \times 10^4$	1.4×10^{-3}
	120 h	$(9.34 + 0.08) \times 10^{-5}$	0.86	$(7.03 + 4.23) \times 10^3$	$(2.82 + 0.72) \times 10^{-4}$	0.59	$(1.24 + 0.27) \times 10^4$	1.5×10^{-3}
LDH-A6	1 h	$(6.54 + 1.65) \times 10^{-5}$	0.89	$(4.95 + 2.59) \times 10^4$	$(7.29 + 3.30) \times 10^{-5}$	0.60	$(3.92 + 0.18) \times 10^4$	1.8×10^{-3}
	4 h	$(8.17 + 3.54) \times 10^{-5}$	0.85	$(2.76 + 1.28) \times 10^4$	$(7.08 + 9.76) \times 10^{-4}$	0.78	$(2.77 + 1.88) \times 10^4$	1.6×10^{-3}
	8 h	$(8.47 + 3.11) \times 10^{-5}$	0.85	$(2.09 + 1.15) \times 10^4$	$(2.30 + 2.51) \times 10^{-4}$	0.74	$(1.85 + 1.14) \times 10^4$	1.7×10^{-3}
	24 h	$(8.69 + 1.60) \times 10^{-5}$	0.86	$(9.98 + 6.49) \times 10^3$	$(1.83 + 0.36) \times 10^{-4}$	0.67	$(1.89 + 0.26) \times 10^4$	2.4×10^{-3}
	48 h	$(9.18 + 2.12) \times 10^{-5}$	0.86	$(7.92 + 3.64) \times 10^3$	$(2.69 + 1.65) \times 10^{-4}$	0.61	$(1.77 + 0.73) \times 10^4$	1.6×10^{-3}
	72 h	$(1.02 + 0.24) \times 10^{-4}$	0.84	$(5.82 + 0.85) \times 10^3$	$(3.25 + 2.30) \times 10^{-4}$	0.59	$(1.93 + 0.98) \times 10^4$	1.3×10^{-3}
	96 h	$(1.06 + 0.25) \times 10^{-4}$	0.83	$(6.06 + 0.79) \times 10^3$	$(3.55 + 3.02) \times 10^{-4}$	0.57	$(2.10 + 1.21) \times 10^4$	1.2×10^{-3}
	120 h	$(1.10 + 1.92) \times 10^{-4}$	0.82	$(7.50 + 2.11) \times 10^3$	$(4.17 + 3.31) \times 10^{-4}$	0.65	$(1.53 + 0.69) \times 10^4$	1.6×10^{-3}

As can be observed from Table 1, R_{ct} of the blank sample increased slightly during the immersion period of 120 h, which was due to the accumulation of the corrosion products. Y_{dl} showed an increasing trend, while n_{dl} demonstrated a decreasing trend, indicating that the electrode surface was becoming gradually heterogeneous due to the development of the corrosion process [26,27]. The R_{ct} values of the LDH-1 were higher than those of the blank sample. The addition of LDH samples effectively enhanced the corrosion resistance of carbon steel. A decrease in R_{ct} and R_f can be observed in the case of LDH-1 with no inhibitor modification after 8 h, which was caused by the fact that the passive film caused by high alkalinity became partially broken due to the decrease in pH. In addition, Y_f also increased and n_f decreased, and Y_{dl} and n_{dl} presented the same trend, demonstrating that a more heterogeneous surface was formed during immersion.

According to Table 2, R_f and R_{ct} values of aspartate-intercalated samples LDH-A1, LDH-A2, LDH-A3, LDH-A4, LDH-A5 and LDH-A6 decreased slightly upon the immersion time with some fluctuations, and the decrease was less than that in the case of LDH-1 without inhibitor intercalation. In addition, Y_f increased and n_f decreased, and Y_{dl} and n_{dl} presented a similar trend, demonstrating that the surface was becoming rougher and the corrosion protection ability of the film on the surface declined gradually.

Polarization resistance R_p is the sum of R_f and R_{ct}, which can be regarded as an indicator to characterize the corrosion resistance of carbon steel [30,31]. Figure 7c presents the variation in R_p of carbon steel in NaCl solutions without and with the addition of 5 g/L LDH-1 and LDH-A1, respectively. It can be seen that the R_p values of carbon steel in blank NaCl solutions were almost more than one order of magnitude lower than those of other samples. Furthermore, the sample in solution with LDH-1 presented significantly lower values than the samples in solution with most of the LDH samples intercalated with aspartates. The sample with LDH-A3 addition demonstrated the largest R_p values, suggesting that N_2 protection was probably able to improve the corrosion protection ability due to the increase in the inhibitor loading amount since CO_2 contamination was almost avoided in this case. In addition, the sample with LDH-A1 addition followed that with LDH-A3 addition, which was higher than those of other samples, indicating that control of other parameters including pH and post-hydrothermal treatment was not of great significance for the final corrosion protection property of LDH. Notably, the one-step solution-mixing method and a fast titration rate in co-precipitation would have a negative influence on the corrosion protection of LDH, probably due to insufficient reaction.

Figure 9 shows optical images of carbon steel after immersion in 0.1 mol/L NaCl solution for 120 h without and with LDH-1 and LDH-A1 additions. It can be seen that the surface of the carbon steel after immersion in blank NaCl solutions was corroded seriously, and lots of porous corrosion products were formed. As for the sample with LDH-1 and LDH-A1 additions, the carbon steel surface remained intact, and no corrosion area can be observed. These results were in good accordance with the changes in R_p during immersion in Figure 7c. Although the R_p values of the sample with LDH-1 were lower than those of the sample with LDH-A1, no remarkable differences can be found in the surface optical characterization. It can be concluded that LDH-1 and LDH-A1 could provide a good corrosion protection effect for carbon steel in 0.1 mol/L NaCl solution during the immersion period.

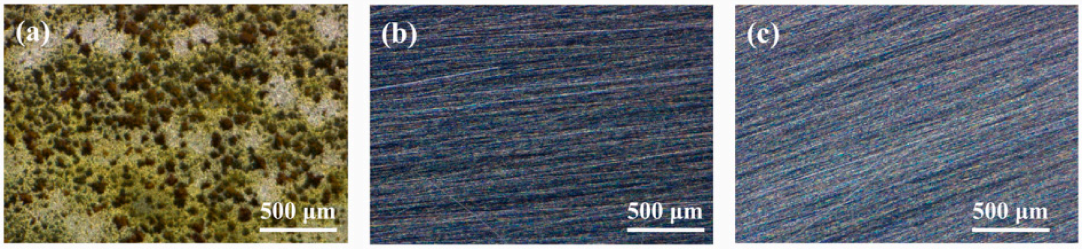


Figure 9. The optical images of the carbon steel after immersion in 0.1 mol/L NaCl solution for 120 h (**a**) with no LDH addition, (**b**) with addition of 5 g/L LDH-1 and (**c**) with addition of 5 g/L LDH-A1.

4. Conclusions

In this work, the influence of preparation parameters on CaAl-LDH was systematically investigated. The effects of solution-mixing mode, reaction atmosphere, pH of the reaction solution, titration rate and hydrothermal post-treatment on the crystalline structure, morphology and chemical composition of LDH were explored, and the influence of variations in these preparation processes on the corrosion inhibition performance of LDH was also studied. The main conclusions are as follows:

(1) For LDH prepared under a nitrogen atmosphere or via a one-step solution-mixing synthesis procedure, less carbonate contamination could be obtained, and, thus, carbonates would account for a lower percentage of the intercalated anions in the LDH gallery. In addition, the one-step solution-mixing synthesis procedure could negatively influence the formation of LDH and, thus, lead to a decrease in the crystallinity of LDH, probably due to insufficient reaction, while hydrothermal post-treatment could increase the crystallinity of LDH by promoting the continual growth of LDH platelets. In addition, the one-step solution-mixing synthesis procedure could lead to the presence of irregular platelets, while post-hydrothermal treatment was able to increase its size, and other parameter variation such as reaction atmosphere, pH of the reaction solution and titration rate would not have an obvious influence on the morphology of LDH.

(2) The results of the anti-corrosion performance tests indicated that adoption of N_2 protection would be helpful for the corrosion protection improvement in inhibitor-intercalated LDH, probably due to the fact that fewer carbonates were intercalated in the LDH gallery; thus, more space would appear for the inhibitor intercalation. In addition, pH control and post-hydrothermal treatment would have little influence on the final corrosion protection ability, while the one-step solution-mixing method and a larger titration rate would be disadvantageous for the corrosion protection effect, probably due to insufficient reaction.

In conclusion, N_2 protection was suggested in the preparation, while the adoption of N_2 protection or not would depend on the relationship between the corrosion protection effect and the intercalated inhibitors. If a small change in the amount of the intercalated

inhibitor could lead to a significant change in the corrosion protection property of LDH, N_2 protection would be of great significance. In addition, sufficient reaction during preparation was also very important due to the fact that insufficient reaction in the one-step solution-mixing method or adoption of a larger titration rate have an obviously negative influence on its corrosion protection ability. In future work, more effort should be devoted to the investigation of the influence of the parameter changes on inhibitor loading, which will be of great significance on its long-lasting corrosion protection effect.

Author Contributions: J.W.: Writing—original draft, investigation, resources, methodology, project administration. S.L.: Writing—original draft, investigation, data curation. K.C.: Writing—review and editing, supervision. Y.C.: Writing—review and editing, supervision, funding acquisition, conceptualization. L.M.: Supervision, conceptualization. D.Z.: Methodology, supervision. All authors have read and agreed to the published version of the manuscript.

Funding: The work was financially supported by the National Natural Science Foundation of China (52301108), the Youth Talent Support Project of China Association for Science and Technology (MK250903), Eagle Plan for Young Elite Talent of Fujian Province (RC266901), Xiamen Municipal Major Science and Technology Program (3502Z20231049) and Science and Technology Innovation Project of Luoyang Ship Material Research Institute (LW246906).

Data Availability Statement: Data will be shared upon request.

Conflicts of Interest: The authors declare no conflicts of interest.

Abbreviations

The following abbreviations are used in this manuscript:

LDH	Layered Double Hydroxide
MOF	Metal–organic Framework
GO	Graphene Oxide
SEM	Scanning Electron Microscope
FTIR	Fourier-Transform Infrared Spectroscopy
XRD	X-ray Diffraction
EIS	Electrochemical Impedance Spectroscopy

References

1. Liu, J.; Fang, Y.; Ou, Y.; Shi, X.; Zhang, Y.; Chen, Q.; Li, L.; Zhou, F.; Liu, W. Synergistic anti-corrosion and anti-wear of epoxy coating functionalized with inhibitor-loaded graphene oxide nanoribbons. *J. Mater. Sci. Technol.* **2025**, *220*, 140–149. [CrossRef]
2. He, X.; Weng, Q.; Guo, R.; Zhang, L.; Sheng, X.; Xie, D. Elaborate construction of potent antioxidant properties in PBP-Ce(III) nanosheets via a one-pot approach for seamless integration of anti-corrosion, wear-resistance, and flame-retardancy. *J. Mater. Sci. Technol.* **2024**, *201*, 197–209. [CrossRef]
3. Li, H.; Meng, X.Z.; Yan, H.J.; Zheng, R.C.; Hu, H.S.; Lei, B.; Zhang, Q.H.; Wu, L.K.; Cao, F.H. Intelligent marine waterborne epoxy coating based on functionalized multiscale nanocomposite: Mechanical enhancement, self-reporting, and active/passive anti-corrosion. *J. Mater. Sci. Technol.* **2025**, *221*, 68–83. [CrossRef]
4. Leng, X.; Yu, H. Graphene-coated hollow glass microspheres modified waterborne epoxy zinc rich anticorrosive coatings. *Paint. Coat. Ind.* **2025**, *55*, 1–7.
5. Wu, Y.; Zhao, C.; Zhao, W. DL@Ti3C2T enhanced waterborne epoxy coating with superior active/passive anti-corrosion properties under 30 MPa hydrostatic pressure. *Corros. Commun.* **2025**, *20*, 1–12. [CrossRef]
6. He, X.; Li, S.; Shen, R.; Ma, Y.; Zhang, L.; Sheng, X.; Chen, Y.; Xie, D.; Huang, J. A high-performance waterborne polymeric composite coating with long-term anti-corrosive property based on phosphorylation of chitosan-functionalized Ti3C2Tx MXene. *Adv. Compos. Hybrid Mater.* **2022**, *5*, 1699–1711. [CrossRef]
7. Jin, Z.; Zhao, Z.; Zhao, T.; Liu, H.; Liu, H. One-step preparation of inhibitor-loaded nanocontainers and their application in self-healing coatings. *Corros. Commun.* **2021**, *2*, 63–71. [CrossRef]

8. Liu, H.; Xu, W.; Ren, H.; Li, D.; He, J.; Xia, L.; Xu, Y.; Zeng, B.; Yuan, C.; Dai, L. Integrated comprehensive protection coating achieved by ligand engineering modulated MXene@LDH heterojunction with anti-corrosion, electromagnetic wave absorption and fire safety. *Chem. Eng. J.* **2024**, *486*, 150444. [CrossRef]
9. Cao, L.; Piao, J.; Wang, W.; Fan, W.; Han, D.; Pei, Y.; Chen, Y.; Zhang, Y. Co-Al hydrotalcite assembled nanofibers to enhance corrosion inhibition and effective Cl− adsorption for long-term corrosion protection. *Chem. Eng. J.* **2024**, *495*, 153052. [CrossRef]
10. Ma, J.; Chang, M.; He, H.; Wei, H.; Huang, Y.; Du, X.; Chen, D. Corrosion Resistance of Li-Al LDHs Film Modified by Methionine for 6063 Al Alloy in 3.5 wt.% NaCl Solution. *Coatings* **2022**, *12*, 507. [CrossRef]
11. Ran, Y.; Ding, J.; Yang, F.; Bao, Q.; Zhu, J.; Du, C.; Tao, P.; Wang, X.; Zhang, S.; Yin, W. A novel organic-inorganic composite flame-retardant coating with excellent compatibility provides superior flame retardancy and smoke suppression for wood. *Ind. Crops Prod.* **2025**, *224*, 120286. [CrossRef]
12. Zhou, L.; Zhang, Q.; Feng, X.; Rui, Z.; Guo, W.; Zhang, Y.; Li, W.; Li, Z. Chloride ion-responsive active protection epoxy composite coatings realized by 2-Mercaptobenzimidazole and 2-Mercaptobenzothiazole intercalated Mg-Al layered double hydroxides. *Corros. Sci.* **2024**, *234*, 112144. [CrossRef]
13. Chen, M.; Wu, F.; Yu, L.; Cai, Y.; Chen, H.; Zhang, M. Chloride binding capacity of LDHs with various divalent cations and divalent to trivalent cation ratios in different solutions. *CrystEngComm* **2019**, *21*, 6790–6800. [CrossRef]
14. Cao, Y.; Wang, J.; Chen, K.; Zhang, X.; Zhang, B.; Fang, S.; Liang, Y.; Huang, C.; Wang, X. A Comparative Study of Chloride Adsorption Ability and Corrosion Protection Effect in Epoxy Coatings of Various Layered Double Hydroxides. *Coatings* **2022**, *12*, 1631. [CrossRef]
15. Tabish, M.; Zhao, J.; Wang, J.; Anjum, M.J.; Qiang, Y.; Yang, Q.; Mushtaq, M.A.; Yasin, G. Improving the corrosion protection ability of epoxy coating using CaAl LDH intercalated with 2-mercaptobenzothiazole as a pigment on steel substrate. *Prog. Org. Coat.* **2022**, *165*, 106765. [CrossRef]
16. Wang, J.; Cao, Y.; Xue, J.; Zhang, X.; Liang, Y.; Chen, K.; Huang, C.; Zheng, D. A comparative experimental and theoretical calculation study of CaAl-LDH modified with various aromatic inhibitors for corrosion protection study in epoxy coatings. *Corros. Sci.* **2024**, *231*, 111994. [CrossRef]
17. Cristoforetti, A.; Parola, F.; Parrino, F.; Izquierdo, J.; Souto, R.M.; Rossi, S.; Deflorian, F.; Fedel, M. Sebacate intercalated Ca Al layered double hydroxide pigments for corrosion protection of low carbon steel: Anion exchange and electrochemical properties. *Appl. Clay Sci.* **2024**, *250*, 107300. [CrossRef]
18. Li, J.; Wang, D.; Hou, L.; Zhang, S.; Wu, P.; Zhang, Y.; Liu, B.; Wei, Y. Enhancing the corrosion resistance of the epoxy coating using CaAl LDH intercalated with L-cysteine and its derivatives as a pigment on steel substrate. *Prog. Org. Coat.* **2024**, *193*, 108527. [CrossRef]
19. Liu, T.; Liu, Y.; Qu, D.; Chen, W.; Qiu, Z.; Qiu, X.; Zhu, L.; Chen, M. Multifunctional epoxy coatings reinforced with LDHs-modified silica microspheres: Synergistic effects on corrosion resistance, thermal insulation, and flame retardancy. *Colloids Surf. A Physicochem. Eng. Asp.* **2024**, *698*, 134578. [CrossRef]
20. Rezaeifard, S.; Shahrabi, T.; Ramezanzadeh, B. Emerging Mo-doped MgAl-LDH lamellar/carbon nanotubes as 3D sustainable nanohybrid for designing a durable smart anti-corrosion composite. *Surf. Coat. Technol.* **2024**, *488*, 131013. [CrossRef]
21. Zhu, J.; Lan, S.; Zhu, D. Functionalized LDH via intercalation of gluconate anion and surface assembly of ultrafine copper hydroxide for improving mechanical properties and the fire safety of epoxy resin. *Appl. Surf. Sci.* **2025**, *680*, 161458. [CrossRef]
22. Ding, C.; Wu, J.; Liu, Y.; Sheng, X.; Cheng, X.; Xiong, X.; Zhao, W. A Waterborne Epoxy Composite Coating with Smart Corrosion Resistance Based on 2-Phenylbenzimidazole-5-sulfonic Acid/Layered Double Hydroxide Composite. *Molecules* **2023**, *28*, 5199. [CrossRef] [PubMed]
23. Liu, A.; Gu, H.; Geng, Y.; Wang, P.; Gao, S.; Li, S. Hydrothermal Synthesis of CaAl-LDH Intercalating with Eugenol and Its Corrosion Protection Performances for Reinforcing Bar. *Materials* **2023**, *16*, 2913. [CrossRef] [PubMed]
24. Li, A.; Xu, W.; Chen, R.; Liu, Y.; Li, W. Fabrication of zeolitic imidazolate frameworks on layered double hydroxide nanosheets to improve the fire safety of epoxy resin. *Compos. Part A* **2018**, *112*, 558–571. [CrossRef]
25. Dai, X.; Wu, L.; Ci, W.; Yao, W.; Yuan, Y.; Xie, Z.; Jiang, B.; Wang, J.; Andrej, A.; Pan, F. Dual self-healing effects of salicylate intercalated MgAlY-LDHs film in-situ grown on the micro-arc oxidation coating on AZ31 alloys. *Corros. Sci.* **2023**, *220*, 111285. [CrossRef]
26. Gao, G.; Liang, C.H.; Wang, H. Synthesis of tertiary amines and their inhibitive performance on carbon steel corrosion. *Corros. Sci.* **2007**, *49*, 1833–1846. [CrossRef]
27. Lin, B. Effect of $[NO_2^-]/[Cl^-]$ Ratio on Corrosion Behavior of Fine- grain High-strength Reinforcement in Simulated Concrete Pore Solutions. *Int. J. Electrochem. Sci.* **2016**, *11*, 3824–3842. [CrossRef]
28. Chen, M.; Yuan, H.; Qin, X.; Wang, Y.; Zheng, H.; Yu, L.; Cai, Y.; Liu, Q.; Liu, G.; Li, W. Improve corrosion resistance of steel bars in simulated concrete pore solution by the addition of EDTA intercalated CaAl-LDH. *Corros. Sci.* **2024**, *226*, 111636. [CrossRef]

29. Alshammari, O.A.O.; Abdelwahab, A.; Jeilani, Y.A.; Ashmawy, A.M.; Deyab, M.A. Electrochemical and quantum chemical exploration on L-ornithine L-aspartate as a sustainable corrosion inhibitor for AISI 1018 steel in acidic environment. *Sci. Rep.* **2026**, *16*, 13029. [CrossRef] [PubMed]
30. Tourabi, M.; Nohair, K.; Traisnel, M.; Jama, C.; Bentiss, F. Electrochemical and XPS studies of the corrosion inhibition of carbon steel in hydrochloric acid pickling solutions by 3,5-bis(2-thienylmethyl)-4-amino-1,2,4-triazole. *Corros. Sci.* **2013**, *75*, 123–133. [CrossRef]
31. Liu, M.; Cheng, X.; Li, X.; Zhou, C.; Tan, H. Effect of carbonation on the electrochemical behavior of corrosion resistance low alloy steel rebars in cement extract solution. *Constr. Build. Mater.* **2017**, *130*, 193–201. [CrossRef]

Disclaimer/Publisher's Note: The statements, opinions and data contained in all publications are solely those of the individual author(s) and contributor(s) and not of MDPI and/or the editor(s). MDPI and/or the editor(s) disclaim responsibility for any injury to people or property resulting from any ideas, methods, instructions or products referred to in the content.